in the presence and absence of 300 μM extracellular Ba^{2+}. Current–voltage relations for transfected and control neurons were calculated by recording whole-cell currents under voltage clamp. Voltage steps in 10-mV increments were applied every 1 s. Evoked synaptic currents were recorded using pipettes whose internal solution was supplemented with QX-314 (4 mM), and in the presence of 50–100 μM picrotoxin in the extracellular medium to isolate excitatory synapses. Brief 1-ms pulses were applied to the entire field of neurons using platinum wires separated by about 5 mm. The applied voltage was systematically varied for each recording until the response amplitude became saturated, indicating reliable activation of all axons innervating the recorded neuron. Responses were measured at a holding potential of −70 mV. To record action-potential firing, without perturbing the intracellular environment, we used the cell-attached patch-clamp method. Pipettes similar to those for whole-cell recordings were used, and tight seals were obtained without break-in. Current recordings (under voltage clamp at −70 mV) allowed unambiguous discrimination of spikes with high signal-to-noise ratios.

FM4-64 imaging

To identify functional presynaptic terminals, we labelled recycling synaptic vesicles using 10 μM FM4-64 (Molecular Probes). Neurons were depolarized for 60 s using hyperkalaemic solution (in mM): 78.5 NaCl, 60 KCl, 10 HEPES, 10 D-glucose, 2 $CaCl_2$, 1.3 $MgCl_2$, 0.05 AP5 (D(-)-2-amino-5-phosphonovaleric acid), 0.005 CNQX (6-cyano-7-nitroquinoxaline-2,3-dione), and 0.001 TTX. Coverslips were then washed in regular extracellular medium without FM4-64 for 10 min before imaging to reduce the background fluorescence caused by non-internalized dye binding to the cell membrane. This protocol has been shown to provide an estimate of the total recycling pool of vesicles. Cells were then imaged in dye-free buffer containing blockers. Earlier experiments also included a de-staining step to release dye from vesicles, and images after de-staining were subtracted from the initial image. As the initial fluorescence and releasable fluorescence were strongly correlated, in most experiments we skipped the de-staining step. Image stacks (Z steps of 1 μm, 7–10 steps) were obtained using a confocal microscope (Olympus Fluoview attached to a BX50WI, × 40, 0.8NA water lens). EGFP and FM4-64 signals were acquired simultaneously using 488-nm excitation, and 510–550-nm band pass and 585 long-pass emission filters, respectively. Transmitted light images were taken separately to identify cell bodies and processes of non-transfected neurons. We chose to measure the density of presynaptic terminals in the proximal regions of the dendrites (about 100 μm from the soma) as these could be identified unequivocally by the EGFP fluorescence. Image analysis was performed in a blind manner with respect to Kir2.1 and mutKir2.1 neurons. Individual puncta were identified manually after thresholding the images using a value that was 2 standard deviations above the background fluorescence. Analysis of fluorescence intensities was performed with custom-written routines in the MATLAB software environment[26].

Analysis

The values for all variables reported were estimated for each cell and averaged across all cells in each group. Errors are reported as standard error of the mean. The Kolmogorov–Smirnoff test was used for all statistical comparisons.

Received 16 July; accepted 23 October 2002; doi:10.1038/nature01242.

1. Turrigiano, G. G. & Nelson, S. B. Hebb and homeostasis in neuronal plasticity. *Curr. Opin. Neurobiol.* **10,** 358–364 (2000).
2. Abbott, L. F. & Nelson, S. B. Synaptic plasticity: taming the beast. *Nature Neurosci.* **3 Suppl.,** 1178–1183 (2000).
3. Katz, L. C. & Shatz, C. J. Synaptic activity and the construction of cortical circuits. *Science* **274,** 1133–1138 (1996).
4. Rao, A. & Craig, A. M. Activity regulates the synaptic localization of the NMDA receptor in hippocampal neurons. *Neuron* **19,** 801–812 (1997).
5. Turrigiano, G. G., Leslie, K. R., Desai, N. S., Rutherford, L. C. & Nelson, S. B. Activity-dependent scaling of quantal amplitude in neocortical neurons. *Nature* **391,** 892–896 (1998).
6. Liao, D., Zhang, X., O'Brien, R., Ehlers, M. D. & Huganir, R. L. Regulation of morphological postsynaptic silent synapses in developing hippocampal neurons. *Nature Neurosci.* **2,** 37–43 (1999).
7. Sanes, J. R. & Lichtman, J. W. Development of the vertebrate neuromuscular junction. *Ann. Rev. Neurosci.* **22,** 389–442 (1999).
8. Crowley, J. C. & Katz, L. C. Development of ocular dominance columns in the absence of retinal input. *Nature Neurosci.* **2,** 1125–1130 (1999).
9. Hubener, M. & Bonhoeffer, T. Eyes wide shut. *Nature Neurosci.* **2,** 1043–1045 (1999).
10. Lin, D. M. *et al.* Formation of precise connections in the olfactory bulb occurs in the absence of odorant-evoked neuronal activity. *Neuron* **26,** 69–80 (2000).
11. Zheng, C., Feinstein, P., Bozza, T., Rodriguez, I. & Mombaerts, P. Peripheral olfactory projections are differentially affected in mice deficient in a cyclic nucleotide-gated channel subunit. *Neuron* **26,** 81–91 (2000).
12. Zhao, H. & Reed, R. R. X inactivation of the OCNC1 channel gene reveals a role for activity-dependent competition in the olfactory system. *Cell* **104,** 651–660 (2001).
13. Luscher, C., Nicoll, R. A., Malenka, R. C. & Muller, D. Synaptic plasticity and dynamic modulation of the postsynaptic membrane. *Nature Neurosci.* **3,** 545–550 (2000).
14. Bi, G. Q. & Poo, M. M. Synaptic modification by correlated activity: Hebb's postulate revisited. *Ann. Rev. Neurosci.* **24,** 139–166 (2001).
15. Davis, G. W. & Bezprozvanny, I. Maintaining the stability of neural function: a homeostatic hypothesis. *Annu. Rev. Physiol.* **63,** 847–869 (2001).
16. Johns, D. C., Marx, R., Mains, R. E., O'Rourke, B. & Marban, E. Inducible genetic suppression of neuronal excitability. *J. Neurosci.* **19,** 1691–1697 (1999).
17. Holt, J. R. *et al.* Functional expression of exogenous proteins in mammalian sensory hair cells infected with adenoviral vectors. *J. Neurophysiol.* **81,** 1881–1888 (1999).
18. Xia, Z., Dudek, H., Miranti, C. K. & Greenberg, M. E. Calcium influx via the NMDA receptor induces immediate early gene transcription by a MAP kinase/ERK-dependent mechanism. *J. Neurosci.* **16,** 5425–5436 (1996).
19. Craig, A. M., Blackstone, C. D., Huganir, R. L. & Banker, G. Selective clustering of glutamate and GABA receptors opposite synaptic terminals releasing the corresponding neurotransmitters. *Proc. Natl Acad. Sci. USA* **91,** 12373–12377 (1994).
20. O'Brien, R. J. *et al.* The development of excitatory synapses in cultured spinal neurons. *J. Neurosci.* **17,** 7339–7350 (1997).
21. Gomperts, S. N., Carroll, R., Malenka, R. C. & Nicoll, R. A. Distinct roles for ionotropic and metabotropic glutamate receptors in the maturation of excitatory synapses. *J. Neurosci.* **20,** 2229–2237 (2000).
22. Cottrell, J. R., Dube, G. R., Egles, C. & Liu, G. Distribution, density, and clustering of functional glutamate receptors before and after synaptogenesis in hippocampal neurons. *J. Neurophysiol.* **84,** 1573–1587 (2000).
23. Balice-Gordon, R. J. & Lichtman, J. W. Long-term synapse loss induced by focal blockade of postsynaptic receptors. *Nature* **372,** 519–524 (1994).
24. Betz, W. J. & Bewick, G. S. Optical analysis of synaptic vesicle recycling at the frog neuromuscular junction. *Science* **255,** 200–203 (1992).
25. Li, Z. & Murthy, V. N. Visualizing post-endocytic traffic of synaptic vesicles at hippocampal synapses. *Neuron* **31,** 593–605 (2001).
26. Murthy, V. N., Schikorski, T., Stevens, C. F. & Zhu, Y. Inactivity produces increases in neurotransmitter release and synapse size. *Neuron* **32,** 673–682 (2001).
27. Bacci, A. *et al.* Chronic blockade of glutamate receptors enhances presynaptic release and downregulates the interaction between synaptophysin-synaptobrevin-vesicle-associated membrane protein 2. *J. Neurosci.* **21,** 6588–6596 (2001).
28. Paradis, S., Sweeney, S. T. & Davis, G. W. Homeostatic control of presynaptic release is triggered by postsynaptic membrane depolarization. *Neuron* **30,** 737–749 (2001).
29. Liao, D., Hessler, N. A. & Malinow, R. Activation of postsynaptically silent synapses during pairing-induced LTP in CA1 region of hippocampal slice. *Nature* **375,** 400–404 (1995).
30. Isaac, J. T. R., Nicoll, R. A. & Malenka, R. C. Evidence for silent synapses: implications for the expression of LTP. *Neuron* **15,** 427–434 (1995).

Supplementary Information accompanies the paper on *Nature*'s website (http://www.nature.com/nature).

Acknowledgements We thank E. Marban for the gift of the EGFP–IRES–Kir2.1 construct. We also thank the members of our laboratory for discussion. This work was supported by grants from the National Institutes of Health and the NSF. V.N.M. is a Sloan Foundation Fellow, a Pew Scholar, an EJLB Foundation Scholar and a National Alliance for Research on Schizophrenia and Depression (NARSAD) Young Investigator. J.B. is a Grable Investigator of NARSAD.

Competing interests statement The authors declare that they have no competing financial interests.

Correspondence and requests for materials should be addressed to V.N.M. (e-mail: vnmurthy@fas.harvard.edu).

Functional improvement of dystrophic muscle by myostatin blockade

Sasha Bogdanovich*†, Thomas O. B. Krag*†, Elisabeth R. Barton*, Linda D. Morris*, Lisa-Anne Whittemore‡, Rexford S. Ahima§ & Tejvir S. Khurana*

** Department of Physiology and Pennsylvania Muscle Institute, University of Pennsylvania School of Medicine, 3700 Hamilton Walk, Richards A-601, Philadelphia, Pennsylvania 19104-6085, USA*
‡ Musculoskeletal Sciences Department, Wyeth Research, Cambridge, Massachusetts 02140, USA
§ Division of Endocrinology, University of Pennsylvania School of Medicine, Philadelphia, Pennsylvania 19104, USA
† These authors contributed equally to this work

Mice[1,2] and cattle[3] with mutations in the myostatin (GDF8) gene show a marked increase in body weight and muscle mass, indicating that this new member of the TGF-β superfamily is a negative regulator of skeletal muscle growth. Inhibition of the myostatin gene product is predicted to increase muscle mass and improve the disease phenotype in a variety of primary and secondary myopathies. We tested the ability of inhibition of myostatin *in vivo* to ameliorate the dystrophic phenotype in the *mdx* mouse model of Duchenne muscular dystrophy (DMD)[4–8].

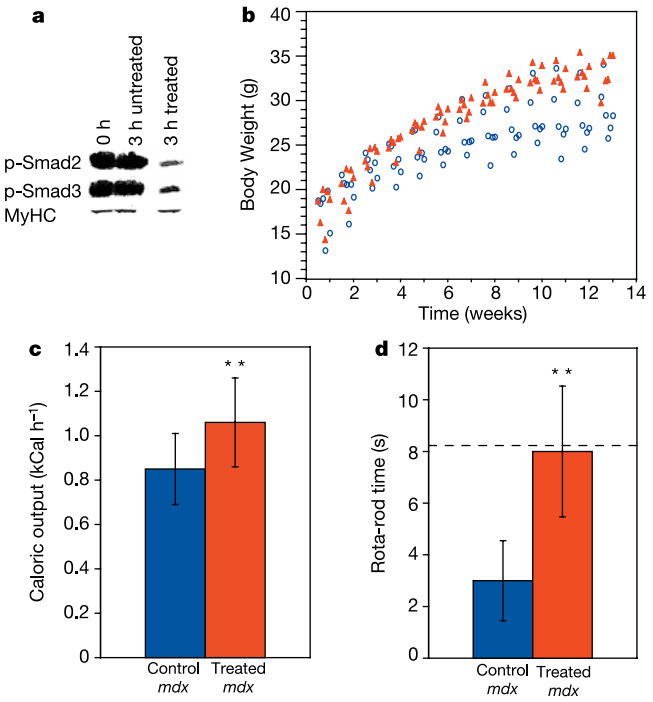

Figure 1 Metabolic consequences of myostatin blockade *in vivo* in *mdx* mice. **a**, Treated C_2C_{12} cells express less phospho-Smad 2 and 3 than PBS treated controls (lower panel shows MyHC control for even loading and transfer). **b**–**d**, Comparison of body weights (**b**), caloric output (**c**) and endurance time (**d**) on a Rota-Rod apparatus between treated *mdx* mice and control *mdx* mice. Treated mice (red) had significantly increased body weight (33.11 ± 2.08 versus 28.99 ± 2.94 g; $n = 12$; $P < 0.03$), caloric output (1.06 ± 0.20 versus 0.85 ± 0.16 kCal h^{-1}; $n = 4$; $P < 0.01$) and endurance time (8 ± 2.5 versus 3 ± 1.5 s; $n = 6$; $P < 0.002$) than controls (blue).

Blockade of endogenous myostatin by using intraperitoneal injections of blocking antibodies for three months resulted in an increase in body weight, muscle mass, muscle size and absolute muscle strength in *mdx* mouse muscle along with a significant decrease in muscle degeneration and concentrations of serum creatine kinase. The functional improvement of dystrophic muscle by myostatin blockade provides a novel, pharmacological strategy for treatment of diseases associated with muscle wasting such as DMD, and circumvents the major problems associated with conventional gene therapy in these disorders.

Cultured C_2C_{12} muscle cells were treated with blocking antibodies generated against myostatin[9,10] to investigate the signalling mechanism of myostatin in muscle. Treated cells had decreased concentrations of phospho-Smad 2 and 3 compared with controls (Fig. 1a). Alterations in Smad 2 and 3 phosphorylation would be predicted to regulate the formation of Smad complexes, their nuclear translocation and transcriptional regulation of genes associated with commitment of muscle progenitors[11,12].

To test myostatin blockage *in vivo*, 4-week-old male *mdx* mice were treated with weekly intraperitoneal injections of blocking antibodies (dose 60 mg kg^{-1}; treated *mdx* group), and vehicle alone (control *mdx* group) for 3 months. Animals were weighed weekly and growth curves were plotted. Treated mice gained weight faster than controls and weighed significantly more than controls after 3 months of treatment (Fig. 1b), which is consistent with the predicted biological effect of myostatin blockade *in vivo*.

To estimate energy expenditure in live animals, we performed indirect calorimetry[13]. Treated mice had a greater caloric output than controls (Fig. 1c), which is consistent with an increase in muscle mass and body size due to myostatin blockade. To determine whether the increase was functional, we used a Rota-rod to assess whole body muscle strength. *Mdx* mice have previously been shown to have an impaired ability to maintain grip and suspend themselves against gravity on the Rota-rod[14]. Treated mice performed better than controls (Fig. 1d), which is consistent with increased functional muscle mass and intact neuromuscular coordination *in vivo*.

To quantify the increase of muscle mass, animals were killed and extensor digitorum longus (EDL) muscles were dissected out and weighed. EDL muscles from treated mice weighed significantly more than those from controls (Fig. 2a). Interestingly, the degree of gain of muscle mass was greater than the degree of increase in body weight (Fig. 2b), suggesting that myostatin blockade had a greater proportional effect on muscle than on other organ systems of *mdx* mice. Weights of other muscles including gastrocnemius, tibialis anterior and quadriceps were similarly increased (data not shown). We quantified functional improvement by analysing physiological properties of muscle (Table 1). Treated mice had significantly increased force production during twitch and tetanic contraction (Fig. 2c–f). This increase in muscle strength was proportional to the degree of increase in muscle mass and offers physiological evidence for a functional improvement in *mdx* muscle produced by myostatin blockade *in vivo*.

To determine whether the increase in muscle mass and strength occurred because of hypertrophy or hyperplasia we performed morphometric examination of the EDL muscle (Table 1). Significant increases were noted in whole-muscle cross-sectional area (CSA) and single-fibre area of EDL from the treated mice, indicating true hypertrophy at the single-myofibre level. Frequency histograms of single-fibre areas revealed an overall shift of distribution towards larger areas (Fig. 2g). No significant difference was noted in the number of muscle fibres, total number of nuclei or the nuclei/fibre ratio in either group, suggesting that the increase in muscle mass and size occurred as a result of hypertrophy and not hyperplasia, as has been noted in dominant-negative myostatin mice[2]. A slight increase was noted in the number of centrally nucleated fibres (CNF) in treated mice, indicating fibres that had undergone either regeneration and/or changes in the state of progenitor cell commitment[8,15]. Because CNF are considered to be more resistant to necrosis[16], their greater proportion might be mechanistic in the improvement in muscle function noted in this study. Interestingly, increased regeneration and/or myogenesis in extraocular muscles has recently been suggested as an important mechanism for the

Table 1 **Comparison of physiological and morphometric properties of EDL muscle**

	C57BL/10	Control *mdx*	Treated *mdx*
CSA (mm^2)	1.4 ± 0.6 (5)	1.5 ± 0.5 (12)	2.0 ± 0.4 (12)**
Absolute force (mN)	356.3 ± 126.8 (10)	370.7 ± 66.5 (12)	491.2 ± 56.5 (12)**
Specific force (mN mm^{-2})	152.6 ± 58.0 (10)	138.1 ± 30.5 (12)	141.5 ± 22.9 (12)
ECC force decrease (1–5) (%)	n.d.	40.0 ± 11.9 (7)	39 ± 4.6 (7)
CNF (%)	3.5 ± 1.3 (1,554)	41.6 ± 10.3 (4,661)	53.4 ± 3.8 (4,711)**
Single-fibre area (μm^2)	n.d.	1,055.0 ± 578.6 (4,661)	1,321.9 ± 785.1 (4,711)**
Number of myofibres	n.d.	786.2 ± 167.0 (6)	777.8 ± 124.1 (6)
Number of nuclei	n.d.	2,266 ± 339.6 (6)	2158 ± 1,058.3 (6)

Results are presented as means ± s.d.; numbers in parentheses are *n*; asterisks, statistical significance ($P \leq 0.05$). CSA, cross-sectional area; ECC, Eccentric contraction; CNF, centrally nucleated fibres; n.d., not determined.

clinical and pathological sparing of this muscle group in DMD[17,18].

To examine for histological evidence of improvement, we sectioned the diaphragm in addition to EDL, because the diaphragm rather than EDL shows degeneration and fibrosis by 16 weeks[19]. Histological analysis revealed insufficient foci of degeneration in EDLs of either group to allow comment on whether improvement had occurred (data not shown). However, diaphragm from treated mice (Fig. 3b) showed a decrease in degenerative changes and cellular infiltration compared with controls (Fig. 3a). The inset in Fig. 3b shows diaphragm from normal C57BL/10 mice for comparison. Immunohistochemistry (Fig. 3c) revealed normal concentrations of utrophin enrichment at the synaptic regions of the muscle, suggesting that myostatin blockade ameliorated the dystrophic phenotype via a utrophin-independent mechanism[20,21]. No differences in utrophin expression were detected by immunoblotting either (data not shown). To ascertain improvement in the pathological status of the whole skeletal musculature, we analysed serum creatine kinase (CK). Elevated CK concentrations are consistently noted with dystrophin deficiency in *mdx* mice and humans owing to sarcolemmal damage[4,22]. At the start of the trial both groups had marked elevations of serum CK compared with normal C57BL/10 mice. However, after 3 months of myostatin blockade *in vivo* there was a marked decline in serum CK concentrations in treated mice (Fig. 3d), to almost normal. These decreases in muscle degeneration and serum CK offer histological and biochemical evidence for a functional improvement in *mdx* muscle produced by myostatin blockade *in vivo*.

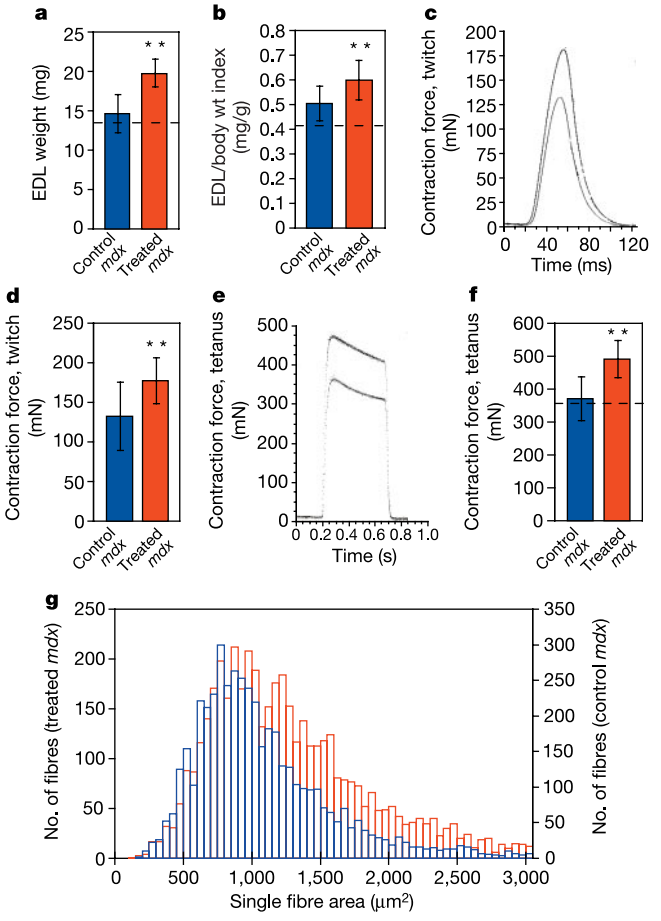

Figure 2 Increase in muscle mass and strength by myostatin blockade. Comparisons of EDL weight (**a**), EDL/body weight index (**b**), twitch force (**c**, **d**), tetanic force (**e**, **f**) and single-fibre areas (**g**), between treated *mdx* mice (red) and control *mdx* mice (blue). Treated mice had significantly increased EDL weight (19.72 ± 1.76 versus 14.63 ± 2.42 mg; $n = 12$; $P < 0.0001$), had an increased EDL/body weight index (0.6 ± 0.08 versus 0.5 ± 0.07; $n = 12$; $P < 0.014$), generated greater twitch force (**c**, representative traces; **d**; 177.32 ± 28.95 versus 132.38 ± 43.07 mN; $n = 12$; $P < 0.03$) and tetanic force (**e**, representative traces; **f**, 491.23 ± 56.54 versus 370.74 ± 66.47 mN; $n = 12$; $P < 0.003$), and had larger single-fibre area distribution (**g**), than controls.

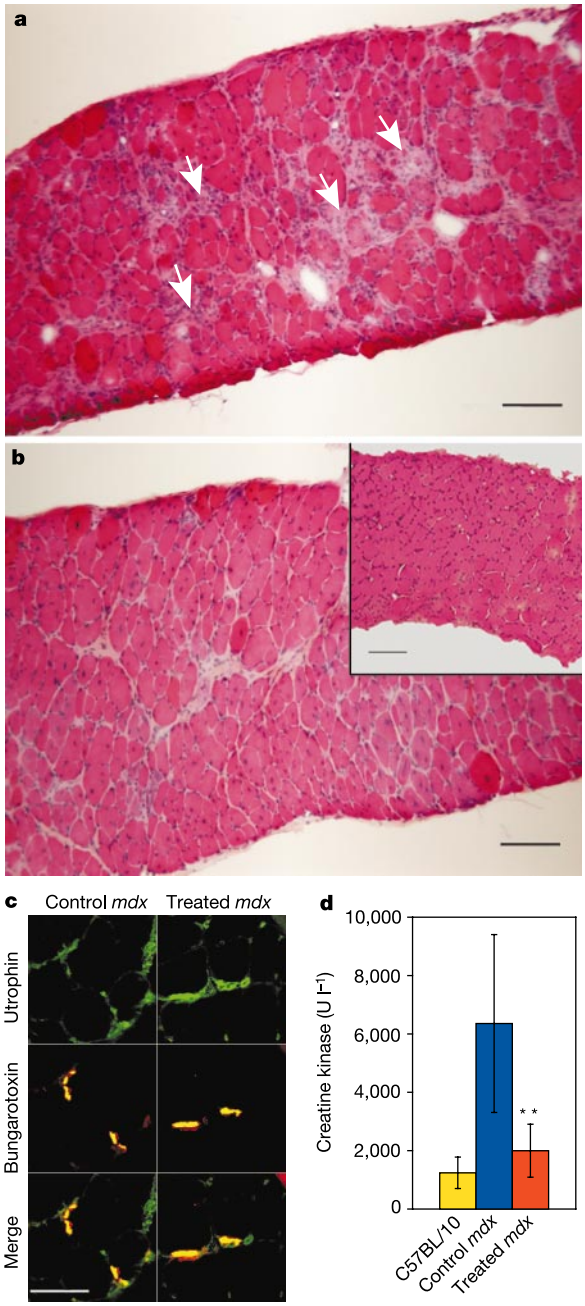

Figure 3 Decreased muscle damage resulting from myostatin blockade. **a**, **b**, Control *mdx* mice (**a**) had significantly greater pathological changes (arrowheads) in the diaphragm than treated mice (**b**), as evidenced by a lack of cellular infiltration and fibrosis. Inset, normal C57BL/10 mice. Haematoxylin–eosin staining; scale bar, 100 μm. **c**, Treated mice (right panels) show no increase in utrophin compared with controls (left panels). Synapses revealed by bungarotoxin staining. Scale bar, 50 μm. **d**, Treated mice (red) had significantly decreased CK concentrations compared with controls (blue; 1997.3 ± 907.37 versus 6356.9 ± 3046.57 U l^{-1}; $n = 6$; $P < 0.005$). The decrease approached C57BL/10 concentrations (yellow; 1241.07 ± 539.77 U l^{-1}; $n = 4$).

Here we have demonstrated that myostatin blockade *in vivo* in *mdx* mice achieved by pharmacological means resulted in a functional improvement of the dystrophic phenotype, by anatomical, physiological and biochemical criteria. The regimen did not completely reverse dystrophic changes; physiological parameters evaluated by *ex vivo* tests, such as susceptibility to damage by lengthening contractions[23,24] were not improved. This might be related to initiating myostatin blockade 1 month after birth rather than at birth, an inadequate dosage, or an inherent limitation of the strategy itself. The nature of the improvement indicates that myostatin blockade might be beneficial for a variety of primary and secondary myopathies such as the muscular dystrophies, ageing and muscle loss due to chronic infections or immobilization. Additionally, it might prove to be a useful adjuvant for the management of systemic metabolic disorders such as obesity and diabetes mellitus[25]. In comparison with conventional transgenic, cell and gene therapy approaches[26–28], the current study used a pharmacological approach (administration of a blocking antibody) to improve the dystrophic phenotype functionally. Delivery of blocking antibodies by simple parenteral injections circumvents the need for the generation of specialized viral vectors to deliver gene products. Furthermore, our approach should obviate the problems concerning toxicity or immune response against the vector, which has been of concern in recent therapeutic trials using conventional gene therapy[29,30]. □

Methods

Physiological studies on isolated muscle

Physiological properties of muscle were analysed with intact *ex vivo* muscle from 16-week-old male *mdx* (C57BL/10ScSn-*DMD*^{mdx}/J) mice, as described previously[23,24]. In brief, muscle length was adjusted to achieve maximal twitch response, and this length (L_0) was measured with vernier calipers. Eccentric contraction (ECC) force decrease was calculated from the difference of isometric force generation during the first and fifth tetanus of the standard ECC protocol (supramaximal stimulus of 700 ms, 500 ms isometric phase, 200 ms eccentric phase; total lengthening L_0/10; lengthening velocity 0.5 $L_0\,s^{-1}$). At the end of physiological studies, muscles were flash-frozen in isopentane cooled in liquid nitrogen, and stored at −80 °C before being sectioned.

Antibodies and histology

The mouse anti-myostatin monoclonal blocking antibody (clone JA16; Wyeth Research/Genetics Institute) was generated against recombinant myostatin and inhibits the binding of myostatin to its receptor ActRIIB with a half-maximal inhibitory concentration of 500 nM (refs 9, 10, 12). Serial frozen sections (7–12 μm thick) were cut at mid-belly of muscle. Sections were examined after haematoxylin–eosin staining or labelling with anti-laminin antibodies and DNA-binding dye Hoechst 33825 for quantifying nuclear content and other morphological indices. Scion Image 4.02 software (http://www.scioncorp.com) was used for morphometric measurements. All cross-sectional myofibres (9,372) and nuclei (26,551) contained in one EDL per animal that was physiologically evaluated in this study were imaged, scored and measured to calculate histological parameters. Affinity-purified BH 11 antibody against utrophin[20,21] (1 μg ml^{-1}), rhodamine-conjugated bungarotoxin (4 μg ml^{-1}; Molecular Probes) and Alexa Fluor® 488 secondary antibodies (Molecular Probes) were used for immunohistochemistry.

Immunoblotting

Cultured C_2C_{12} cells were treated with anti-myostatin antibody (11.5 μl ml^{-1}) for 3 h and controls were treated with PBS. Cells were harvested in sample buffer, resolved by SDS–polyacrylamide gel electrophoresis and electrotransferred to poly(vinylidene difluoride) membrane. Efficiency of transfer and the even loading of lanes was verified by using post-transfer Ponceau S staining of the membrane. Membranes were probed with antibodies specific against phospho-Smad 2 and 3 (Santa Cruz Biotechnology) and antibody complexes detected using enhanced chemiluminescence (Pierce).

Biochemical and functional assessment of muscle

Serum CK was measured with the indirect CK colorimetric assay kit and standards (Sigma). The Rota-rod apparatus was designed and built in the laboratory (details available from the authors on request). The apparatus consisted of a hollow plastic rod 6 mm in diameter attached horizontally to a direct-current motor. Rotation speed was calibrated to 18 r.p.m. by using a potentiometer and stopwatch. Indirect calorimetry was performed with the Oxymax Equalflow system (Columbus Instruments). Mice were acclimatized to the test chamber on a 12–h light–dark cycle (light on at 0700h) for 2 days, and night-time energy expenditure was measured at 15-min intervals. Settings used per cycle were as follows: airflow, 500 ml min^{-1}; sample flow, 400 ml min^{-1}; settle time, 120 s; measuring time, 60 s; temperature, 22 °C. The caloric output (kCal h^{-1}) was calculated as 3.815 + 1.232 × respiratory exchange ratio (RER). RER is the ratio between carbon dioxide generated and oxygen consumption.

Statistical analysis

Student's *t*-test was used for determining statistical significance throughout the study. Graphical representation of data uses the following convention: mean ± s.d.; treated *mdx* mice in red; control *mdx* mice in blue; dashed line represents data from age-matched C57BL/10 normal mice.

Received 10 July; accepted 16 September 2002; doi:10.1038/nature01154.

1. McPherron, A. C., Lawler, A. M. & Lee, S. J. Regulation of skeletal muscle mass in mice by a new TGF-β superfamily member. *Nature* **387,** 83–90 (1997).
2. Zhu, X., Hadhazy, M., Wehling, M., Tidball, J. G. & McNally, E. M. Dominant negative myostatin produces hypertrophy without hyperplasia in muscle. *FEBS Lett.* **474,** 71–75 (2000).
3. Grobet, L. *et al.* A deletion in the bovine myostatin gene causes the double-muscled phenotype in cattle. *Nature Genet.* **17,** 71–74 (1997).
4. Bulfield, G., Siller, W. G., Wight, P. A. & Moore, K. J. X chromosome-linked muscular dystrophy (mdx) in the mouse. *Proc. Natl Acad. Sci. USA* **81,** 1189–1192 (1984).
5. Torres, L. F. & Duchen, L. W. The mutant mdx: inherited myopathy in the mouse. Morphological studies of nerves, muscles and end-plates. *Brain* **110,** 269–299 (1987).
6. Hoffman, E. P., Monaco, A. P., Feener, C. C. & Kunkel, L. M. Conservation of the Duchenne muscular dystrophy gene in mice and humans. *Science* **238,** 347–350 (1987).
7. Hoffman, E. P., Brown, R. H. Jr & Kunkel, L. M. Dystrophin: the protein product of the Duchenne muscular dystrophy locus. *Cell* **51,** 919–928 (1987).
8. Coulton, G. R., Morgan, J. E., Partridge, T. A. & Sloper, J. C. The mdx mouse skeletal muscle myopathy. I. A histological, morphometric and biochemical investigation. *Neuropathol. Appl. Neurobiol.* **14,** 53–70 (1988).
9. Thies, R. S. *et al.* GDF-8 propeptide binds to GDF-8 and antagonizes biological activity by inhibiting GDF-8 receptor binding. *Growth Factors* **18,** 251–259 (2001).
10. Jalenak, M. *et al.* Transcriptional changes arising from in vivo inhibition of myostatin. *J. Neurol. Sci.* **199** (suppl)., S83 (2002).
11. Moustakas, A., Souchelnytskyi, S. & Heldin, C. H. Smad regulation in TGF-beta signal transduction. *J. Cell Sci.* **114,** 4359–4369 (2001).
12. Lee, S. J. & McPherron, A. C. Regulation of myostatin activity and muscle growth. *Proc. Natl Acad. Sci. USA* **98,** 9306–9311 (2001).
13. Guyton, A. C. *Textbook of Medical Physiology* (W. B. Saunders, New York, 1995).
14. Muntoni, F., Mateddu, A., Marchei, F., Clerk, A. & Serra, G. Muscular weakness in the mdx mouse. *J. Neurol. Sci.* **120,** 71–77 (1993).
15. Brown, S. C. & Lucy, J. A. *Dystrophin: Gene, Protein and Cell Biology* (Cambridge Univ. Press, Cambridge, 1997).
16. Matsuda, R., Nishikawa, A. & Tanaka, H. Visualization of dystrophic muscle fibers in mdx mouse by vital staining with Evans blue: evidence of apoptosis in dystrophin-deficient muscle. *J. Biochem. (Tokyo)* **118,** 959–964 (1995).
17. McLoon, L. K. & Wirtschafter, J. D. Continuous myonuclear addition to single extraocular myofibers in uninjured adult rabbits. *Muscle Nerve* **25,** 348–358 (2002).
18. Fischer, M. D. *et al.* Expression profiling reveals metabolic and structural components of extraocular muscles. *Physiol. Genom.* **9,** 71–84 (2002).
19. Stedman, H. H. *et al.* The mdx mouse diaphragm reproduces the degenerative changes of Duchenne muscular dystrophy. *Nature* **352,** 536–539 (1991).
20. Khurana, T. S., Hoffman, E. P. & Kunkel, L. M. Identification of a chromosome 6-encoded dystrophin-related protein. *J. Biol. Chem.* **265,** 16717–16720 (1990).
21. Khurana, T. S. *et al.* Immunolocalization and developmental expression of dystrophin related protein in skeletal muscle. *Neuromuscul. Disord.* **1,** 185–194 (1991).
22. Engel, A. G. & Franzini-Armstrong, C. *Myology* (McGraw-Hill, New York, 1994).
23. Petrof, B. J., Shrager, J. B., Stedman, H. H., Kelly, A. M. & Sweeney, H. L. Dystrophin protects the sarcolemma from stresses developed during muscle contraction. *Proc. Natl Acad. Sci. USA* **90,** 3710–3714 (1993).
24. Moens, P., Baatsen, P. H. & Marechal, G. Increased susceptibility of EDL muscles from mdx mice to damage induced by contractions with stretch. *J. Muscle Res. Cell Motil.* **14,** 446–451 (1993).
25. Ahima, R. S. & Flier, J. S. Leptin. *Annu. Rev. Physiol.* **62,** 413–437 (2000).
26. Tinsley, J. M. *et al.* Amelioration of the dystrophic phenotype of *mdx* mice using a truncated utrophin transgene. *Nature* **384,** 349–353 (1996).
27. Gussoni, E. *et al.* Dystrophin expression in the *mdx* mouse restored by stem cell transplantation. *Nature* **401,** 390–394 (1999).
28. Ebihara, S. *et al.* Differential effects of dystrophin and utrophin gene transfer in immunocompetent muscular dystrophy (mdx) mice. *Physiol Genom.* **3,** 133–144 (2000).
29. Tripathy, S. K., Black, H. B., Goldwasser, E. & Leiden, J. M. Immune responses to transgene-encoded proteins limit the stability of gene expression after injection of replication-defective adenovirus vectors. *Nature Med.* **2,** 545–550 (1996).
30. Lozier, J. N. *et al.* Toxicity of a first-generation adenoviral vector in rhesus macaques. *Hum. Gene Ther.* **13,** 113–124 (2002).

Acknowledgements We thank L. Sweeney, C. Bönnemann, J. Khurana (University of Pennsylvania) and L. Edvinsson (Glostrup Hospital, University of Copenhagen and Lund) for guidance and helpful discussions, and N. Wolfman (Wyeth Research/Genetics Institute) for providing reagents and helpful discussions. T.S.K. was a paid consultant for Wyeth Research/Genetics Institute during the study. The study was supported in part by a grant from Wyeth Research/Genetics Institute and a predoctoral fellowship to T.O.B.K. from the Faculty of Medicine, Copenhagen University, Denmark.

Competing interests statement The authors declare competing financial interests: details accompany the paper on *Nature*'s website (http://www.nature.com/nature).

Correspondence and requests for materials should be addressed to T.S.K. (e-mail: tsk@mail.med.upenn.edu).